J. Appl. Cryst. (1994). **27**, 595–608

Determination of Size Distributions from Small-Angle Scattering Data for Systems with Effective Hard-Sphere Interactions

BY JAN SKOV PEDERSEN

Department of Solid State Physics, Risø National Laboratory, DK-4000 Roskilde, Denmark

(*Received* 5 *October* 1993; *accepted* 9 *December* 1993)

Abstract

Methods for the free-form determination of size distributions for systems with hard-sphere interactions are described. An approximation, called the local monodisperse approximation, is introduced. Model calculations show that this approximation gives relatively small errors even at relatively high polydispersities and large volume fractions. The size distributions are determined by least-squares methods with smoothness and non-negativity constraints. The local monodisperse approximation leads to normal equations that are linear in the amplitude of the size distribution. This is used when solving the least-squares problem: only the two effective parameters describing the interference effects are treated as nonlinear parameters in an external optimization routine. The parameters describing the size distribution are determined by a linear least-squares method. The size distribution is also determined using the nonlinear equations from the calculation of the scattering intensity in the Percus–Yevick approximation. For this, a nonlinear least-squares routine with a smoothness contstraint and a non-negativity constraint is used. Both approaches are tested by analysis of simulated examples calculated by the analytical expressions in the Percus–Yevick approximation. Finally, the methods are applied to two sets of experimental data from silica particles and from δ' precipitates in an Al–Li alloy. For the simulated examples, good agreement is found with the input distributions. For the experimental examples, the results agree with the expected and known properties of the samples.

1. Introduction

Free-form determination of size distributions from small-angle scattering data can be carried out using, for example, various regularization techniques (Glatter, 1980; Svergun, Semenyuk & Feigin, 1988; Potton, Daniell & Rainford, 1988). In the application of these methods, it is assumed that the volume fraction of the particles is small and that interactions between the particles are negligible. However, for many systems these assumptions are not fulfilled. This is the case for most colloidal suspensions with a volume fraction larger than a few percent and also for colloidal suspensions of charged particles [see, for example, Kaler (1988) and Ottewill (1991)]. For these systems, the particle configurations give rise to interference effects in the small-angle scattering data. Another type of system for which interparticle interference effects are important is that of precipitates in metallic alloys [see, for example, Kostorz (1991) and Fratzl (1991)]. In these systems, the positions of the precipitates are correlated as the formation of the precipitates leads to depleted zones around the particles. No other precipitates form in these zones and this gives rise to an effective repulsion between the particles and strong interference effects in the small-angle scattering data. It has recently been shown (Pedersen, 1993*a*) that the small-angle scattering data from spherical δ' particles in Al–Li alloys can be analysed in terms of a polydisperse hard-sphere model. Owing to the depleted zones, the effective hard-sphere interaction radius is larger than the actual radius of the particles. Correlations between the precipitating particles can also be caused by elastic interactions.

Analytical calculations of the small-angle scattering intensity for systems with interactions and polydispersity have only been done for particles with hard-sphere interactions (Vrij, 1979; Blum & Stell, 1979; Salacuse & Stell, 1982). These calculations are done within the Percus–Yevick approximation. The equations for the intensity are quite involved, which is probably the reason for the frequent use of approximations rather than the analytical solutions when experimental data are analysed. The most well known approximation is the 'decoupling approximation', which was introduced by Kotlarchyk & Chen (1983). In this approach, it is assumed that the positions of the particles are independent of their sizes. Furthermore, the interference effects are described by an effective structure factor calculated for the average size of the particles. This structure factor is modified by a term that takes into account the influence of the polydispersity effects on the particle form factors. This approach gives reasonable results for small polydispersities but for larger values it gives large systematic deviations from the analytical results.

In §2.2 of this paper, a new approximation, the *local monodisperse approximation*, is introduced. It is assumed that the positions of the particles are completely correlated with their sizes. That is, the system

is approximated by many subsystems in which the particles are monodisperse. The total scattering is then calculated as the sum of the scattering from the subsystems weighted according to the size distribution of the system. This approach gives a more realistic smearing of the interference effects due to the (approximate) inclusion of the polydispersity of the interaction radius and therefore works better for large polydispersities. In §3, the results from the decoupling approximation and the local monodisperse approximation are compared with the analytical results for the hard-sphere model. The local monodisperse approximation has the further advantage that it gives rise to equations for the scattering intensity that are linearly dependent on the amplitude of the size distribution. It is therefore straightforward to determine a free-form solution for the size distribution by employing regularization methods with a non-negativity constraint. This approach is described in §2.1.

The analytical solution for the scattering intensity for the polydisperse hard-sphere model depends (Vrij, 1979; Blum & Stell, 1979; Salacuse & Stell, 1982) in a highly nonlinear way on the amplitude of the size distribution. In §2.3, an approach is described in which the size distribution obtained from the local monodisperse approximation is used as a first estimate in a nonlinear least-squares optimization of the analytical model. A regularization procedure and a non-negativity constraint are also applied in this approach.

In §4, the two methods are tested by application to several simulated examples. Applications to experimental data are described in §5.

2. Models

2.1. *Infinitely dilute systems*

In this section, the basic equations and methods for the linear least-squares problem are introduced. For simplicity, systems at infinite dilution are considered first, but the descriptions are also valid for systems with higher concentrations when treated in the local monodisperse approximation. In the indirect method of Glatter (1977, 1980), the distribution to be determined is parameterized as a linear combination of a set of basis functions. The number-density size distribution $N(R)$ is written as

$$N(R) = \sum_{n=1}^{N} a_n B_n(R), \tag{1}$$

where a_n are coefficients and $B_n(R)$ are the basis functions, which are usually taken as cubic spline functions. As $N(R)$ is a number-density distribution, it fulfils $N(R) \geq 0$, and this condition should be incorporated in the solution. The cubic spline functions overlap with, in general, six neighbouring functions, which makes the condition $a_n \geq 0$ a much stronger condition than is needed for making the distribution non-negative. Linear spline functions are therefore used in the present work. They are given by

$$B_n(x) = \begin{cases} 1 - |x - n| & \text{for } |x - n| \leq 1 \\ 0 & \text{elsewhere.} \end{cases} \tag{2}$$

These functions overlap only with two neighbours and for $x = n$ the value of the distribution is determined only by the function with index n. Therefore, the biimplication $[B_n(R) \geq 0] \Leftrightarrow (a_n \geq 0)$ holds. These functions give the best resolution for the smallest number of functions in regions where the distribution goes to zero. The small-angle scattering cross section $\mathrm{d}\sigma(q)/\mathrm{d}\Omega$ is given by

$$\frac{\mathrm{d}\sigma}{\mathrm{d}\Omega}(q) = \Delta\rho^2 \int_0^\infty N(R)\Phi(q,R)^2 \mathrm{d}R, \tag{3}$$

where $\Delta\rho$ is the excess scattering-length density of the particles. The modulus of the scattering vector is $q = 4\pi \sin\theta/\lambda_0$, where θ is half the scattering angle and λ_0 is the wavelength of the radiation. In (3), $\Phi(q, R)$ is the form factor of the particle with size R. For spherical particles, it is

$$\Phi(q, R) = 3V_o[\sin(qR) - qR\cos(qR)]/(qR)^3, \tag{4}$$

where V_o is the volume of a sphere with radius R.

Expression (1) for the size distribution is inserted in (3) and the coefficients can be determined by a least-squares method. One minimizes

$$\chi^2 = \sum_{i=1}^{P} [I^{\mathrm{meas}}(q_i) - I^{\mathrm{mod}}(q_i)]^2/\sigma_i^2, \tag{5}$$

where P is the number of points in the measured data set, $I^{\mathrm{meas}}(q_i)$ are the measured intensities, σ_i are the standard errors and $I^{\mathrm{mod}}(q_i)$ are the model intensities given by the cross section (3), smeared by instrumental resolution if necessary [see, for example, Glatter (1977) and Pedersen, Posselt & Mortensen (1990)].

According to the sampling theorem, the resolution in real space is $\Delta R \simeq \pi/q_{\max}$, where $q_{\max}$ is the largest scattering vector probed in the experiment. The resolution of the spline functions describing the distribution is $\Delta R \simeq R_{\max}/N$, where $R_{\max}$ is the upper limit of the support of $N(R)$. From these two expressions for ΔR, one obtains $N \simeq R_{\max} q_{\max}/\pi$. This gives, typically, $N = 10$–40. However, occasionally N has to be larger than the value given by the sampling theorem in order to resolve abrupt changes in $N(R)$ and prevent 'ringing' in the solution. In general, the number of parameters to be determined is so large that the normal equations for the least-squares problem are

ill-conditioned. Therefore, a regularization in terms of a constraint or a stabilizing function has to be used. In the present work, a constraint similar to the smoothness constraint introduced by Glatter (1977, 1980) was used:

$$N_c = \sum_{n=1}^{N-1} (a_{n+1} - a_n)^2 + a_1^2 + a_N^2. \quad (6)$$

This constraint is a measure of the total length of the curve describing the distribution. It has low values for smooth bell-shaped distributions. The expression that has to be minimized is $\chi^2 + \lambda N_c$, where λ is a Lagrangian multiplier, which in the present work was determined by the point-of-inflection method suggested by Glatter (1977). The modified normal equations that have to be solved are similar to those given by Glatter (1977).

Non-negativity of the coefficients was imposed on the solution using the procedure given by Lawson & Hanson (1974) for a linear least-squares problem with linear inequality constraints. During the procedure, the restricted normal equations were solved by the Gauss–Jordan elimination procedure. The procedure given by Lawson & Hanson (1974) has also been applied in the program package of Provencher (1982) and by Schnablegger & Glatter (1991) for determining size distributions from light scattering data.

When the size distribution is determined, a series of characteristic parameters can be calculated. These are most conveniently expressed by the moments $\overline{R^n}$ of the distribution

$$\overline{R^n} = \int_0^\infty R^n N(R) \mathrm{d}R. \quad (7)$$

One has the following characteristic parameters for the size distribution:

$$\langle R \rangle = \overline{R^1}/\overline{R^0}, \quad (8)$$

$$\sigma(R)^2 = \int_0^\infty (R - \langle R \rangle)^2 N(R) \mathrm{d}R / \overline{R^0} \quad (9)$$

and

$$R_{\mathrm{gyr}}^2 = \tfrac{3}{5}\overline{R^8}/\overline{R^6}, \quad (10)$$

which are, respectively, the average radius of the particles, the variance of the distribution and the radius of gyration. One can also directly calculate the volume fraction η of the particles and the specific surface area S:

$$\eta = (4\pi/3)\overline{R^3} \quad (11)$$

and

$$S = 4\pi\overline{R^2}. \quad (12)$$

Errors in all these parameters can be obtained by standard error analysis using the covariance matrix or by a Monte Carlo procedure as described by Svergun & Pedersen (1994). Both of these procedures are implemented in the computer programs and give, for most applications, similar results. The parameters that are fixed at zero by the non-negativity constraint during the fitting procedure are not included in the error calculation.

2.2. *The local monodisperse approximation*

For a given configuration of the particle, one can write the scattering cross section using the Debye equation, which takes into account the interference of the radiation scattered from different particles. The cross section is written as discrete summations over the particles in the sample

$$\frac{\mathrm{d}\sigma}{\mathrm{d}\Omega}(q) = \Delta\rho^2 \sum_{i,j} \{\Phi(q, R_i)\Phi(q, R_j) \times [\sin(qr_{ij})/qr_{ij}]\}, \quad (13)$$

where R_i and R_j are the radii of the particles with indices i and j, respectively, and r_{ij} is their separation. The expression can be rewritten as

$$\begin{aligned}\frac{\mathrm{d}\sigma}{\mathrm{d}\Omega}(q) &= \Delta\rho^2 \Big(\sum_i \Phi(q, R_i)^2 \\ &\quad + \sum_{i,j,i\neq j} \{\Phi(q, R_i)\Phi(q, R_j)[\sin(qr_{ij})/qr_{ij}]\} \Big) \\ &\simeq \Delta\rho^2 \sum_i \Big(\Phi(q, R_i)^2 \Big\{ 1 + \sum_{j,j\neq i} [\sin(qr_{ij})/qr_{ij}] \Big\} \Big),\end{aligned} \quad (14)$$

where, in the last line, the form factor of the jth particle has been replaced by that of the ith. The term inside the curly brackets in the last line is approximated by the structure factor $S(q, R_{\mathrm{HS}}(R_i))$ of the monodisperse hard-sphere model. The interaction radius R_{HS} should be a known function of the radius R. For particles interacting with their actual radius one has $R_{\mathrm{HS}} = R$. The expressions for $S(q, R_{\mathrm{HS}})$ are within the Percus–Yevick approximation (see, for example, Kinning & Thomas, 1984):

$$S(q, R_{\mathrm{HS}}) = [1 + 24\eta_{\mathrm{HS}} G(R_{\mathrm{HS}}q)/(R_{\mathrm{HS}}q)]^{-1}. \quad (15)$$

In this equation, η_{HS} is the volume fraction of the hard spheres and

$$\begin{aligned}G(A) = {} & \alpha(\sin A - A\cos A)/A^2 \\ & + \beta[2A\sin A + (2 - A^2)\cos A - 2]/A^3 \\ & + \gamma\{-A^4\cos A + 4[(3A^2 - 6)\cos A \\ & + (A^3 - 6A)\sin A + 6]\}/A^5,\end{aligned} \quad (16)$$

where

$$\alpha = (1 + 2\eta_{HS})^2/(1 - \eta_{HS})^4$$
$$\beta = -6\eta_{HS}(1 + \eta_{HS}/2)^2/(1 - \eta_{HS})^2 \qquad (17)$$
$$\gamma = \eta_{HS}\alpha/2.$$

By a change to the continuous variables, (14) can be written as

$$\frac{d\sigma}{d\Omega}(q) = \Delta\rho^2 \int_0^\infty \Phi(q, R)^2 S[q, R_{HS}(R)] N(R) dR. \qquad (18)$$

From this equation, it can be seen that the scattering intensity in the present approximation is given as the incoherent sum of the scattering intensities of monodisperse subsystems weighted with the size distribution. Alternatively, one can regard the intensity as originating from a system in which the size of the particles varies slowly with the position in the system so that every particle is surrounded by particles of the same size. Therefore, this approximation is called the *local monodisperse* approximation. It is based on the assumption that the position and the size of the particles are completely correlated. This is opposite to the assumption used in the decoupling approximation, in which the position and the size are assumed to be independent. The local monodisperse approximation gives rise to a smearing of the interparticle interference effects by the polydispersity. Such a smearing is not included in the decoupling approximation, for which the interference effects are described by a monodisperse structure factor calculated for the average-size particles. This is further discussed in §§3 and 6. It should also be mentioned that the local monodisperse approximation can be expected to give a good description of some real systems for which the particle size is correlated with position. This is the case for precipitates in materials near dislocations in Al–Li alloys (Mahalingam, Gu, Liedl & Sanders, 1987) and gas bubbles near dislocations and grain boundaries in metals (Li, Kesternich, Schroeder, Schwahn & Ullmaier, 1990).

When the volume fraction of the hard spheres η_{HS} and the function $R_{HS}(R)$ are specified, the intensity given by (18) is linear in the parameters a_n describing the size distribution. Therefore, the methods described in the previous section can be used to obtain a non-negative solution for $N(R)$. In real applications, the data might contain residual background. In the computer program, an additional independent parameter can be included to describe this. Small-angle scattering data from precipitates in metallic alloys often contain a power-law (q^{-4}) contribution at small q, which originates from large impurities or precipitates. The prefactor of this power-law contribution is also an independent fitting parameter, which can be included in the fitting procedure.

The intensity (18) depends nonlinearly on η_{HS} and R. For precipitates in metallic alloys, local conservation of the precipitating material suggests that the volume of the depletion zone around a precipitate should be proportional to the volume of the precipitates (see, for example, Pedersen, 1993*a*). Therefore, $R_{HS} = CR$, where C is a constant. This gives two nonlinear parameters: η_{HS} and C. In other systems, the interaction radius R_{HS} is given as $R_{HS} = R + \Delta R$, where ΔR is a constant independent of R. This is the case for colloidal particles surrounded by shells of constant thickness with vanishing scattering contrast. In the computer program, the two parameters describing the interference effects (η_{HS}/C or $\eta_{HS}/\Delta R$) can be optimized by a grid or a gradient search (Bevington, 1969) in an external routine. For each value of η_{HS} and C (or ΔR), the linear parameters are determined by the procedure described in §2.1.

The procedure for analysing a data set is as follows. First guesses of η_{HS} and C (or ΔR) are given. For these values, the weight of the smoothness constraint λ is determined by the point-of-inflection method. Then, the values of η_{HS} and C (ΔR) are determined using the value obtained for λ. If the values of η_{HS} and C (ΔR) change significantly, a new optimum value of λ is determined and η_{HS} and C (ΔR) are optimized again. This procedure is continued until λ, η_{HS} and C (ΔR) no longer change significantly. In most applications, the correct value of λ is determined already by the first guess for the values for η_{HS} and C (ΔR). Note that, for systems with an actual hard-sphere interaction, η_{HS} and C (ΔR) are not real physical parameters but should be considered as effective parameters describing the interference effects.

Errors in the size distribution and the parameters that are derived from the size distribution are calculated as described in the previous section, neglecting the variances and covariance connected with the parameters η_{HS} and C (or ΔR).

2.3. *The analytical model*

The scattering cross section for the polydisperse collection of hard spheres has been calculated for an arbitrary size distribution by Vrij (1979), Blum & Stell (1979) and Salacuse & Stell (1982). In the present work, the solution given by Vrij was used. The intensity is obtained by calculating averages of various parameters and functions weighted by the size distribution, *i.e.* moments of R, averages of form factors *etc.*

The size distribution is expressed by (1). The intensity depends strongly nonlinearly on the coefficients and a nonlinear least-squares method has to be applied. Additional (possible) fitting parameters are: a background, a prefactor for a q^{-4} power law, C (or ΔR) and the scattering contrast squared, $\Delta\rho^2$. The values of the size distribution on an absolute scale determine the shape of the scattering curve, whereas $\Delta\rho^2$ determines the intensity values on an absolute scale.

The smoothness constraint (6) was included in the nonlinear least-squares optimization. This gives the following modified normal equations for the change Δa_ν in the parameter a_ν (Pedersen, 1992):

$$\sum_{\nu=1}^{N_p}(\alpha_{\mu\nu}+\lambda K_{\mu\nu})\Delta a_\nu = \beta_\mu - \lambda L_\mu, \qquad \mu = 1,2,\ldots,N_p, \quad (19)$$

where

$$\alpha_{\mu\nu} = \sum_{i=1}^{P}\frac{\partial I^{\mathrm{mod}}}{\partial a_\mu}(q_i)\frac{\partial I^{\mathrm{mod}}}{\partial a_\nu}(q_i)/\sigma_i^2$$

and

$$\beta_\mu = \sum_{i=1}^{P}[I^{\exp}(q_i) - I^{\mathrm{mod}}(q_i)]\frac{\partial I^{\mathrm{mod}}}{\partial a_\mu}(q_i)/\sigma_i^2. \quad (20)$$

When the first N of the N_p parameters are taken to be those describing the size distribution, one has

$$K_{\mu\nu} = \begin{cases} 2 & \text{for } \mu=\nu \text{ and } \nu = 1,\ldots,N \\ -1 & \text{for } \mu=\nu-1 \text{ and } \nu = 2,\ldots,N \\ -1 & \text{for } \mu=\nu+1 \text{ and } \nu = 1,\ldots,N-1 \\ 0 & \text{elsewhere} \end{cases} \quad (21)$$

and

$$L_\nu = \begin{cases} 2a_\nu - a_{\nu+1} & \text{for } \nu = 1 \\ 2a_\nu - a_{\nu+1} - a_{\nu-1} & \text{for } 2 \le \nu \le N-1 \\ 2a_\nu - a_{\nu-1} & \text{for } \nu = N \\ 0 & \text{elsewhere.} \end{cases} \quad (22)$$

The normal equations have to be solved iteratively. In order to solve the normal equations the first time, a set of starting values for the parameters is required. In the applications, these were taken from the fit using the local monodisperse model. In addition, an estimate of the scattering contrast has to be given. The equations are solved using the method of Marquardt (1963). This method combines a gradient search with a linearization of the fitting functions. The iteration procedure is continued until the absolute values of the changes are smaller than a specified limit. The computer code was based on the algorithm given by Press, Flannery, Teukolsky & Vetterling (1989). The non-negativity constraint on the parameters describing the size distribution was included in the search procedure. Parameters that became negative when changed by the amount Δa_ν were instead divided by 10. In combination with the damped search in the Marquardt algorithm, this procedure was found to work reliably.

The procedure to analyse a data set is as follows. First, the size distribution and the additional parameters are determined using the local monodisperse approximation. These values, together with an estimate of the scattering contrast, are used as starting values for fitting the analytical model. First, only the parameter $C = R_{\mathrm{HS}}/R$ or ΔR is fitted, the remaining parameters being kept fixed. This gives reasonable values for this parameter, which allows the rest of parameters to be fitted and the variation of λ to be performed. In most applications, the value of λ is equal to the one obtained for the solution from the local monodisperse approximation.

Errors in the size distribution and the parameters that are derived from the size distribution can be obtained by standard error analysis using the covariance matrix. However, the influence of the non-negativity constraint is neglected in this error calculation and it might give rise to values that are too large. For comparison, a Monte Carlo procedure similar to the one described by Svergun & Pedersen (1994) was also applied. When the fit to the data is determined, a large number (typically 50) of simulated data sets are generated around the original data set. This is done by adding a Gaussian-distributed random error of the same size as the original error of each data point. The changes in the parameters are determined by solution of (19). The left-hand side of the equation is calculated using the values determined by the fit to the original data and is kept fixed. The equations can be solved for all the simulated data sets simultaneously using a Gauss–Jordan elimination procedure. The changes in the parameters are limited so that only positive values are obtained for the parameters. The variance of the changes in the parameters and the variance of the parameters derived from the size distribution are easily obtained and give directly the standard errors in the parameters and the size distribution. In general, the parameters obtained by the Monte Carlo procedure are smaller than those obtained from the covariance matrix.

3. Comparisons of approximations

In this section, results from the local monodisperse approximation are compared with those from the analytical solution of Vrij (1979) and those from the decoupling approximation of Kotlarchyk & Chen (1983). In this latter approximation, the scattering cross section is given by

$$\frac{\mathrm{d}\sigma}{\mathrm{d}\Omega}(q) = \Delta\rho^2\langle\Phi(q,R)^2\rangle S_{\mathrm{eff}}(q), \quad (23)$$

where

$$S_{\mathrm{eff}}(q) = 1 + \overline{\beta(q)}[S(q,\langle R_{\mathrm{HS}}^3\rangle^{1/3}) - 1] \quad (24)$$

with

$$\overline{\beta(q)} = \langle\Phi(q,R)\rangle^2/\langle\Phi(q,R)^2\rangle, \quad (25)$$

where $\langle\,\rangle$ means the first moment with respect to the size distribution and $S(q,R_{\mathrm{HS}})$ is given by (15), (16) and (17).

The model size distribution was chosen as a Gaussian function with centre at R_c and with full width at half-maximum (FWHM) W. (The Gaussians were truncated at $R = 0$.) The scattering intensities were calculated for a series of different examples using the three different approaches. Also, effective structure factors were calculated according to

$$S_{\text{eff}}(q) = \frac{\mathrm{d}\sigma}{\mathrm{d}\Omega}(q)/[\Delta\rho^2\langle\Phi(q,R)^2\rangle]. \qquad (26)$$

The scattering contrast was arbitrarily set to $\Delta\rho^2 = 20 \times 10^{20}\,\text{cm}^{-4}$ in all the calculations. Figs. 1 and 2 show, respectively, the dependence of the scattering intensity and of the effective structure factor for fixed values of the volume fraction $\eta = 0.3$, $C = R_{\text{HS}}/R = 1$, $\Delta R = 0$ and $R_c = 100$ Å at different values of W (see figure captions). One sees in Figs. 1 and 2 that the local monodisperse approximation is significantly better than the decoupling approximation at high polydispersities. It gives a smoother effective structure factor and much better agreement with the analytical results at small scattering vectors. However, significant deviations are present for $W = 100$ Å.

Figs. 3 and 4 show comparisons for different values of η. The rest of the parameters were fixed: $R_c = 100$ Å, $W = 100$ Å, $C = 1$ and $\Delta R = 0$. The local monodisperse approximation gives a better agreement with the analytical results for these examples also. It reproduces reasonably the maxima in the scattering intensities and in the structure factor, but at small scattering vectors the values are underestimated. This effect increases as the volume fraction increases.

The last comparison concerns the variation of the volume fraction of the hard spheres η_{HS} for constant volume fraction η. The fixed parameters are: $\eta = 0.1$, $R_c = 100$ Å, $W = 100$ Å and $\Delta R = 0$. The plots (*a*), (*b*), (*c*) and (*d*) in Figs. 5 and 6 correspond to $\eta_{\text{HS}} = 0.1$, 0.2, 0.3 and 0.4, respectively. The corresponding values of C are 1, 1.2599, 1.4422 and 1.5874, respectively. The local monodisperse approximation gives for this comparison also the best agreement with the analytical results. The agreement gets worse as η_{HS} is increased.

4. Analysis of simulated examples

In this section, the methods described in §2 for determining size distributions using the local monodisperse and the analytical models are examined. The scattering data were generated using the expressions given by Vrij (1979). Random Gaussian-distributed noise of 3% was added to the data. The data were generated for 40 equidistant values of q between 0.003 and 0.06 Å^{-1} and 40 equidistant values between 0.03 and 0.3 Å^{-1}. This corresponds roughly to two instrumental settings of a small-angle neutron scattering instrument.

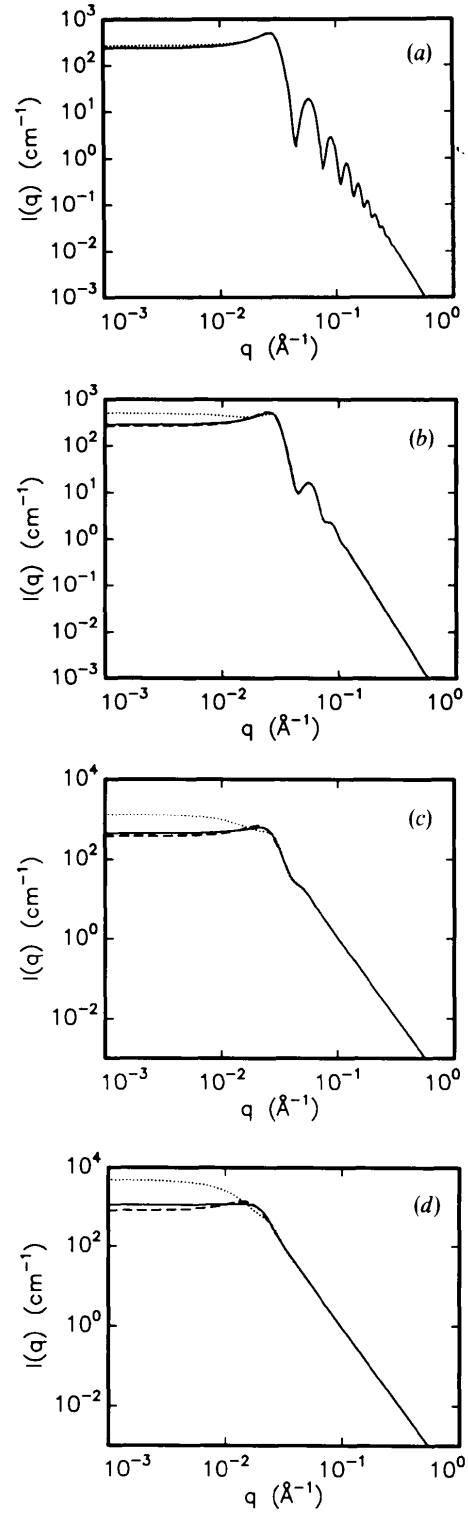

Fig. 1. Comparison of the scattering intensity for a Gaussian size distribution with $R_c = 100$ Å. The FWHM values are (*a*) 10, (*b*) 25, (*c*) 50 and (*d*) 100 Å. $\eta = 0.3$, $C = 1$ and $\Delta R = 0$. Full lines: analytical calculation. Broken lines: local monodisperse approximation. Dotted lines: decoupling approximation. In (*a*), the broken line and the full line coincide.

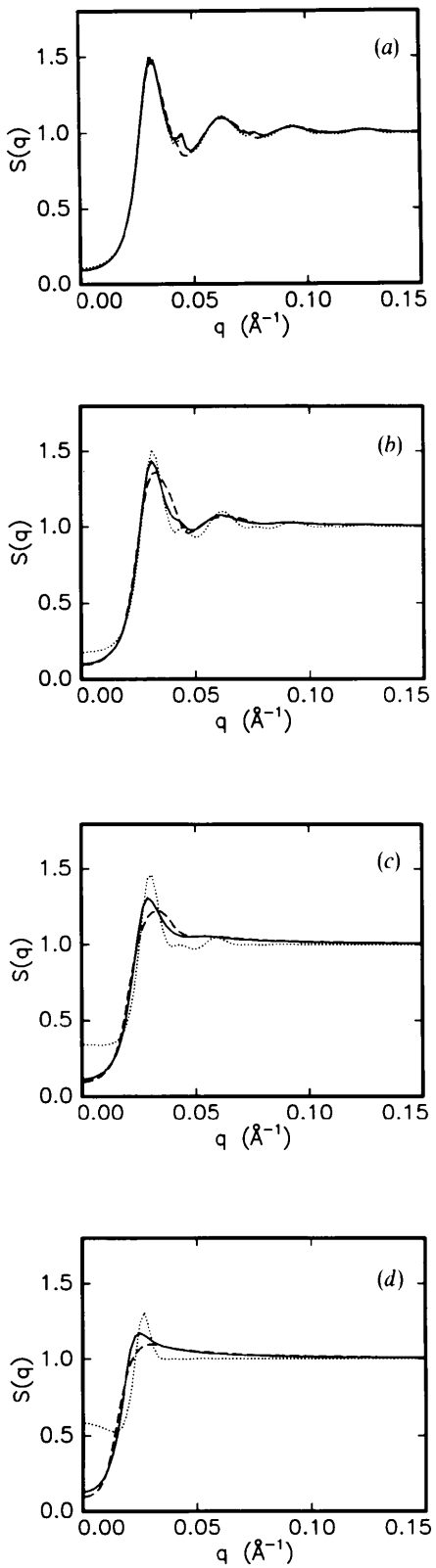

Fig. 2. Comparison of the effective structure factors for the examples shown in Fig. 1. The line styles are the same as in Fig. 1.

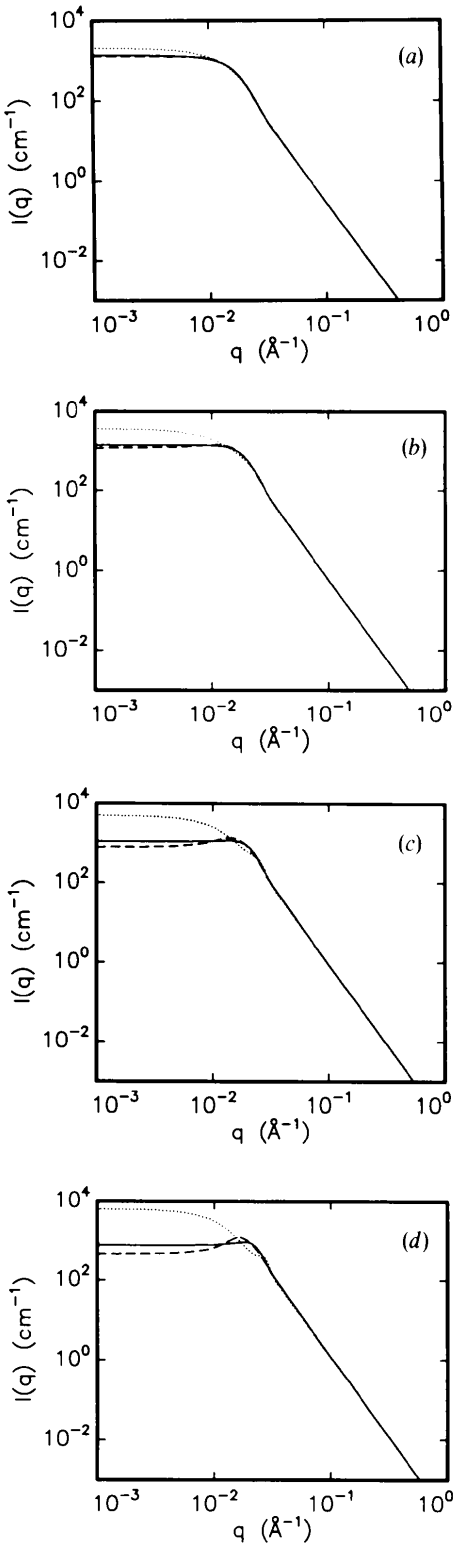

Fig. 3. Comparison of the scattering intensity for a Gaussian size distribution with R_c = 100 Å and W = 100 Å. The values for η are (*a*) 0.1, (*b*) 0.2, (*c*) 0.3 and (*d*) 0.4. The parameter C is fixed at 1 and ΔR is fixed at zero. The line styles are the same as in Fig. 1.

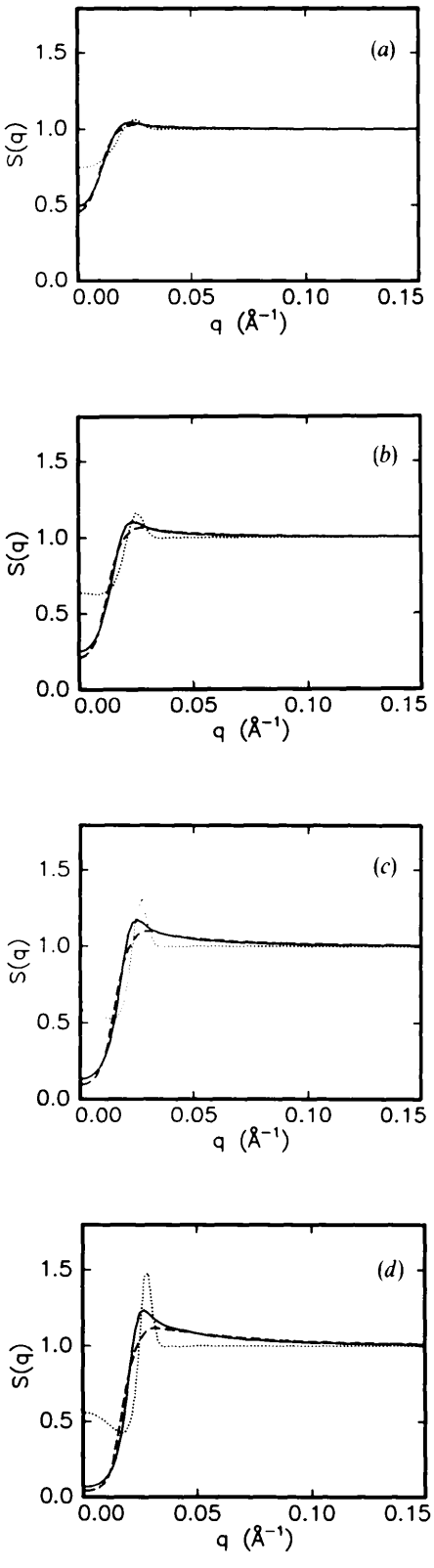

Fig. 4. Comparison of the effective structure factors for the examples shown in Fig. 3. The line styles are the same as in Fig. 1.

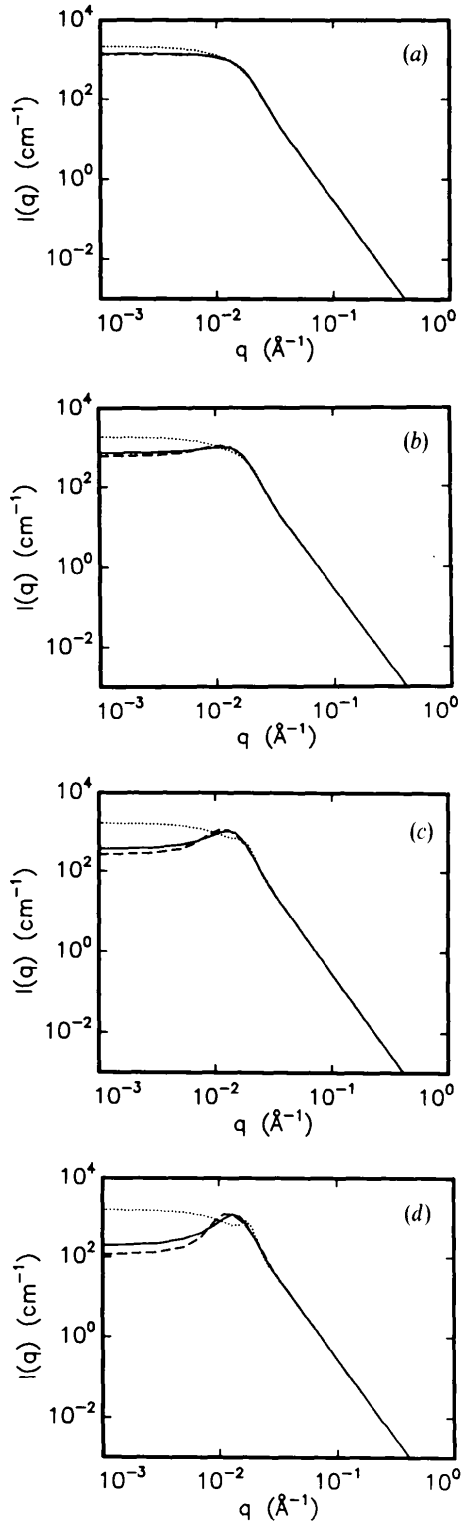

Fig. 5. Comparison of the scattering intensity for a Gaussian size distribution with R_c = 100 Å and W = 100 Å. The volume fraction η is fixed at 0.1 and ΔR = 0. The values for the hard-sphere volume fraction η_{HS} are (*a*) 0.1, (*b*) 0.2, (*c*) 0.3 and (*d*) 0.4. The line styles are the same as in Fig. 1.

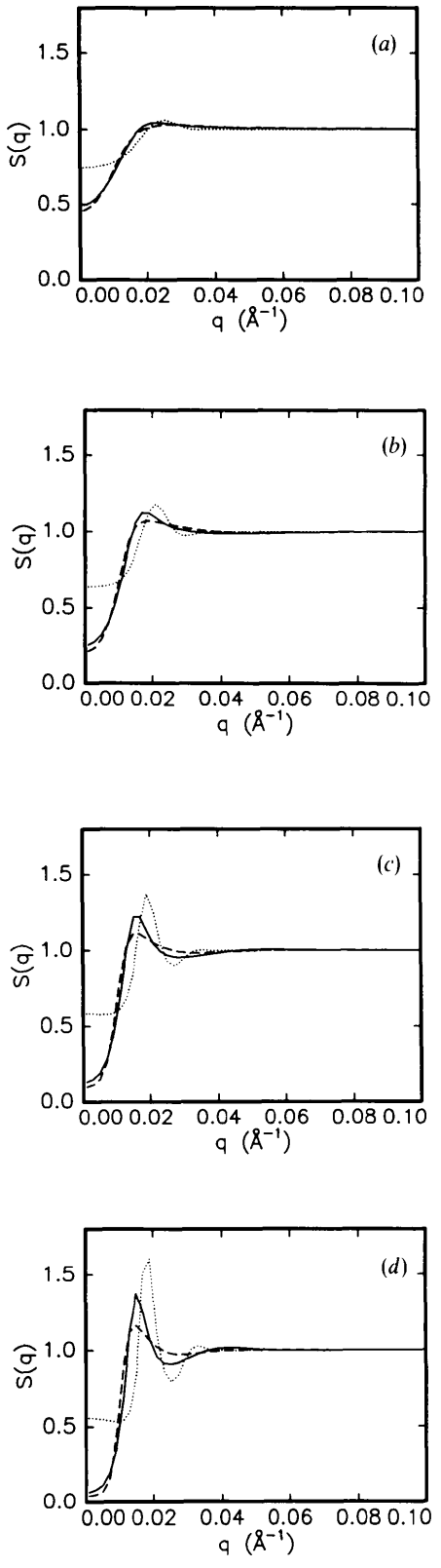

Fig. 6. Comparison of the effective structure factors for the examples shown in Fig. 5. The line styles are the same as in Fig. 1.

Table 1. *Results from the analysis of simulated scattering data for the example shown in Fig. 7(a)*

Parameters	Original	Local monodisperse	Analytical
$\overline{R}$ (Å)	75.00	68.7 (9)	68.3 (19)
$\sigma(R)$ (Å)	30.79	33.6 (3)	33.9 (4)
R_{gyr} (Å)	95.39	95.6 (7)	95.8 (9)
η	0.0001000	0.001008 (4)	0.001013 (17)
S (cm^{-1})	3070.06	3109 (9)	3118 (26)

In order to test the linear and nonlinear methods without taking into account the particle interference effects, an example was generated with a low volume fraction: $\eta = 0.001$, $C = 1$ and $\Delta R = 0$. Also, in the examples in this section the contrast was fixed at $\Delta\rho^2 = 20 \times 10^{20}$ cm^{-4}. The original size distribution (the full curve in Fig. 7*a*) was chosen in order to check the resolution capability of the methods. It consisted of two Gaussians, one with $R_c = 50$ Å and $W = 25$ Å and another with $R_c = 100$ Å and $W = 50$ Å. The amplitudes of the two functions were chosen so that they contained the same number of particles.

The data were analysed as described in §2. The number of spline functions was 20 and the maximum radius R_{max} was 175 Å. The restored size distributions are shown in Fig. 7(*a*). For the local monodisperse approximation, η_{HS} was fixed at zero. As expected, the two methods give identical results for this example. The distributions agree well with the original one for $R >$ 70 Å but show significant deviations at smaller R values. The small particles give a very small contribution to the scattering intensity owing to the weighting by the volume squared through the form factor [(3) and (4)]. The smoothness constraint influences the solution in the low-R region and gives a smearing of the peak around 50 Å. The parameters derived from the size distributions are displayed in Table 1, where the errors estimated by Monte Carlo simulations are also given. The parameters R_{gyr}, η and S are recovered nearly within the estimated errors. The parameters $\overline{R}$ and $\sigma(R)$ are, respectively, underestimated and overestimated owing to the influence of the constraint at small R values.

For the next example (Fig. 7*b*), the size distribution is broad and monomodal, $R_c = 100$ Å and $W = 100$ Å, with a volume fraction of 0.3 and $C = 1$. Owing to the large polydispersity and the relatively high volume fraction, this is an example that is relatively difficult to analyse. For these conditions, the local monodisperse approximation is not expected to give perfect results (see Fig. 1*d*). The number of splines used in the analysis was 20 and $R_{max} = 250$ Å. The distribution determined by the local monodisperse approximation has significant deviations from the original one. It is higher at low R values ($R < 140$ Å) and lower at higher values. The distribution determined by the analytical model agrees

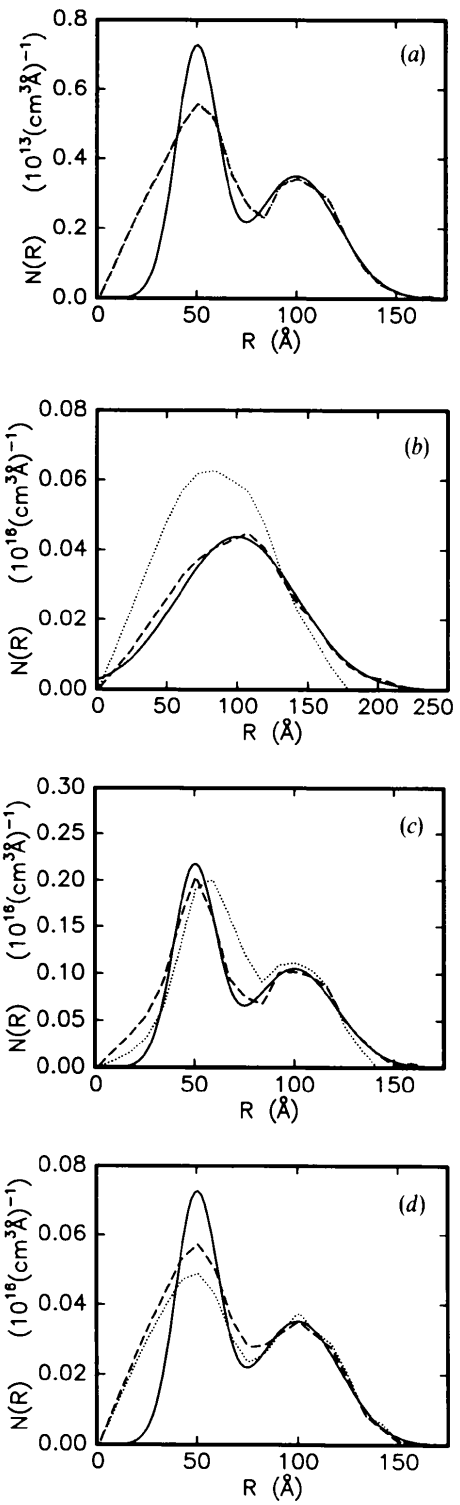

Fig. 7. Size distributions from analysing simulated scattering data. Full curve: original distribution. Dotted curve: distribution from the local monodisperse approximation. Broken curve: distribution from the analytical model. The parameters for the original distributions are: (*a*) $\eta = 0.001$, $C = 1$. (*b*) $\eta = 0.3$, $C = 1$. (*c*) $\eta = 0.3$, $C = 1$. (*d*) $\eta = 0.1$, $C = 1.4422$. For all examples $\Delta R = 0$.

Table 2. *Results from the analysis of simulated scattering data for the example shown in Fig. 7(b)*

The parameters describing the interference effects in the local monodisperse approximation are, after optimization, $C = 1.00$ and $\eta_{HS} = 0.182$.

Parameters	Original	Local monodisperse	Analytical
$\overline{R}$ (Å)	101.03	85.1 (7)	99.4 (16)
$\sigma(R)$ (Å)	29.60	36.1 (2)	41.3 (7)
R_{gyr} (Å)	131.56	107.8 (5)	131.3 (30)
η	0.300	0.258 (1)	0.301 (4)
S (cm^{-1})	690002	693900 (2300)	696000 (3800)

Table 3. *Results from the analysis of simulated scattering data for the example shown in Fig. 7(c)*

The parameters describing the interference effects in the local monodisperse approximation are, after optimization, $C = 0.944$ and $\eta_{HS} = 0.238$.

Parameters	Original	Local monodisperse	Analytical
$\overline{R}$ (Å)	75.00	73.3 (11)	71.5 (16)
$\sigma(R)$ (Å)	30.79	27.7 (6)	32.4 (5)
R_{gyr} (Å)	95.39	87.6 (2)	95.7 (15)
η	0.300	0.295 (1)	0.305 (3)
S (cm^{-1})	921017	956400 (2900)	935500 (5900)

very well with the original one. In Table 2, it can also be seen that the parameters derived from the size distributions agree within the statistical errors with the values derived from the original size distribution. For the local monodisperse approximation, the deviations are typically 15–20%. After optimization, the effective parameters describing the interference effects in the local monodisperse approximation are $C = 1.00$ and $\eta_{HS} = 0.182$. The low hard-sphere volume fraction reflects the overestimation of the interference effects by the approximation for large polydispersities and large volume fractions (Fig. 1*d*).

For the last two examples (Figs. 7*c* and *d*), the original size distributions have shapes similar to the bimodal one in Fig. 7(*a*). For the example shown in Fig. 7(*c*), $\eta = 0.3$ and $C = 1$. In the local monodisperse approximation, the size distribution has some minor deviations from the original one. However, it is clearly seen that the distribution is bimodal. The parameters derived from the distribution deviate by typically less than 10% from the values obtained from the original distribution (Table 3). After optimization, the parameters describing the interference effects are $\eta_{HS} = 0.238$ and $C = 0.944$. The size distribution determined by the analytical model agrees very well with the original one except at small R values where the sensitivity is low. The deviations of the parameters derived from the size distribution have the same magnitude as the statistical errors, *i.e.* a few percent (see Table 3).

For the last example, the volume fraction is $\eta = 0.1$ and $C = 1.4422$, which gives a hard-sphere volume

Table 4. *Results from the analysis of simulated scattering data for the example shown in Fig. 7(d)*

The parameters describing the interference effects are: for the local monodisperse approximation, $C = 1.31$ and $\eta_{HS} = 0.262$; for the analytical model, $C = 1.442$ (4).

Parameters	Original	Local monodisperse	Analytical
$\overline{R}$ (Å)	75.00	69.8 (9)	67.7 (14)
$\sigma(R)$ (Å)	30.79	34.5 (3)	34.4 (5)
R_{gyr} (Å)	95.39	94.6 (5)	97.1 (14)
η	0.1000	0.1022 (5)	0.1010 (11)
S (cm^{-1})	307006	310900 (1200)	310400 (1900)

fraction of $\eta_{HS} = 0.3$. The size distributions (Fig. 7*d*) are in good agreement with the original one for both the local monodisperse and the analytical model, with some smearing of the component around 50 Å. The parameters derived from the size distributions are given in Table 4. The values of R_{gyr}, η and S have deviations from the original values that are of the same size as the statistical errors. The values of $\overline{R}$ and $\sigma(R)$ deviate by about 10% from the original values. These deviations are larger than the statistical errors due to the smearing of the component of the size distribution around 50 Å.

This completes the applications to simulated examples. These examples have shown that both the local monodisperse and the analytical models can be used to obtain information on the size distribution for simulated examples for systems with hard-sphere interactions. In §5, the approaches are applied to real experimental examples taken from the literature.

5. Analysis of experimental examples

The first example concerns small-angle neutron scattering data for a colloidal suspension of silica particles ('SP23') with a volume fraction $\eta \simeq 0.5$ coated with octadecyl chains (de Kruif, Briels, May & Vrij, 1988). The scattering data are shown in Fig. 8(*a*) [note that Figs. 18 and 19 are interchanged in the paper by de Kruif *et al.* (1988)]. The scattering intensities are not given on an absolute scale by de Kruif *et al.* The data analysis requires this and therefore the scattering contrast has to be estimated. With the scale for the scattering data used in the present work, it was found that a scattering contrast of $\Delta\rho = 2.0 \times 10^{10}$ cm^{-2} gave a volume fraction of about 0.50 for the local monodisperse model when the volume fraction was calculated from the size distribution using (11). The instrumental smearing of the model scattering curve was included in the analysis as described by Pedersen, Posselt & Mortensen (1990) and by Pedersen (1993*b*).

The hard-sphere interaction radius is expected to be given by the actual radius R plus a constant ΔR that accounts for a shell describing the grafted octadecyl chains (de Kruif *et al.*, 1988). This was included in the models in which ΔR is a fitting parameter. The size distribution for the local monodisperse model is shown in Fig. 8(*b*). The fit to the data is excellent for the following effective parameters for the interference effects: $\Delta R = -10.2$ Å and $\eta_{HS} = 0.474$. The size distribution from electron microscopy is also shown in Fig. 8(*b*). The amplitude has been rescaled arbitrarily to agree with the size distributions determined from the small-angle scattering data. The parameters derived from the size distributions are given in Table 5. There is good agreement between the parameters.

The size distribution and parameters were used as starting values for the fit of the analytical model. The scattering contrast changed only slightly to $\Delta\rho = 1.964\,(5) \times 10^{10}$ cm^{-2}. The constant thickness of the shell with the octadecyl chains was $\Delta R = 3.8\,(8)$ Å, which is much less than the expected 18 Å (de Kruif *et al.*, 1988). This could be due to either a large flexibility of the chains or the main direction of the chains being parallel to the surface of the particles. The fit to the data is shown in Fig. 8(*a*). It is very good but there

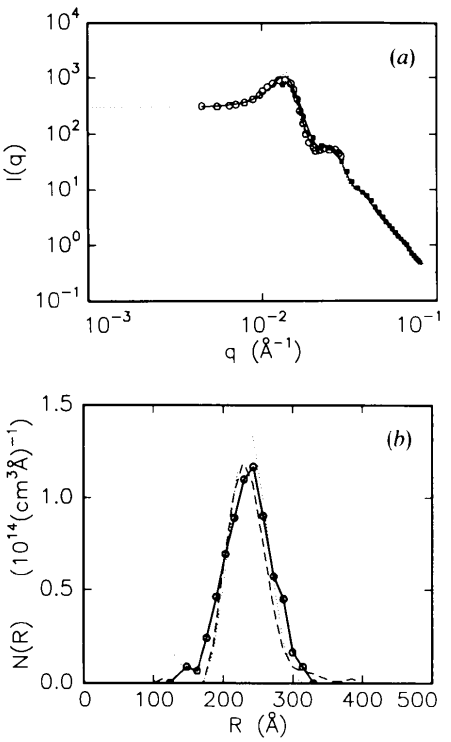

Fig. 8. (*a*) Experimental scattering data from de Kruif *et al.* (1988) for silica particles coated with octadecyl chains. The curves are the fits of the analytical model. The dotted curve is the ideal nonsmeared cross section and the full curves are the cross section smeared by the appropriate resolution functions. (Deviations between the two curves can be seen in the overlap region of the two instrumental settings.) (*b*) The size distributions. The dotted curve is from the local monodisperse model and the broken curve is from the analytical model. The thick full curve with circles in (*b*) is from electron microscopy (de Kruif *et al.*, 1988).

Table 5. *Results from the analysis of experimental scattering data shown in Fig. 8 (de Kruif et al., 1988) for silica particles ('SP23') coated with octadecyl chains*

The parameters describing the interference effects are: for the local monodisperse approximation, $\Delta R = -10.2$ Å and $\eta_{HS} = 0.474$; for the analytical model, $\Delta R = 3.8\,(8)$ Å. The scattering contrast with the normalization used was $\Delta\rho = 2.0 \times 10^{10}$ cm^{-2} for the local monodisperse model and $\Delta\rho = 1.964\,(5) \times 10^{10}$ cm^{-2} for the analytical model. The parameters in the last column are based on the electron-microscopy results given by de Kruif *et al.* (1988).

Parameters	Local monodisperse	Analytical	Electron microscopy
$\overline{R}$ (Å)	231 (1)	237 (17)	235
$\sigma(R)$ (Å)	35 (1)	33 (3)	30
R_{gyr} (Å)	196.1 (3)	216 (5)	203
η	0.525 (3)	0.50 (2)	-
S (cm^{-1})	655000 (3600)	602000 (30000)	-

is a tendency for the correlation peak to be broader in the data than in the model. The size distribution is shown in Fig. 8(*b*). It is very similar to the distributions from the local monodisperse model and from electron microscopy. The most important difference is a small tail of the distribution at large R values. This tail gives rise to a difference of about 10% for the radius of gyration, as can been seen in Table 5. The two other parameters $\overline{R}$ and$\sigma(R)$ are similar to the values from the local monodisperse model and from electron microscopy. The volume fraction is $\eta = 0.50\,(2)$, in excellent agreement with the expected value.

The second and last example concerns the δ' precipitates in the metallic alloy Al–Li. The data are taken from Triolo, Caponetti, Spooner & Boschetti (1989) and are for an Al–2.14 wt%Li alloy aged at 413 K for 4 h. The data are shown in Fig. 9(*a*). The scattering curve shows a pronounced peak originating from the correlations of the precipitates and a q^{-4} tail at low q originating from large impurities. From electron microscopy (Mahalingam *et al.*, 1987), it is known that the precipitates are nearly spherical and that the size distribution is quite broad.

The strong correlation peak in the scattering curve originates from the way the precipitates are formed. Each precipitate contains the nonsoluble lithium from a zone around it. In this zone, no other precipitates can be formed. The resulting spatial distribution of the precipitates therefore corresponds to that of a system with repulsion between the particles. In order for there to be local conservation of the precipitating material, the volume of the depletion zone has to be proportional to the volume of the precipitates. When the repulsion is described by an effective hard-sphere radius of the particles, this radius has to be proportional to the actual radius, as this gives local conservation of the material. Such a hard-sphere model has been shown to be applicable to small-angle scattering data from Al–Li alloys (Pedersen, 1993*a*). In that work, the size distribution was taken to be a Weibull density distribution, as this distribution has been shown to give a good description of the size distribution in Al–Li alloys (Mahalingam *et al.*, 1987).

The size distribution from the local monodisperse model is shown in Fig. 9(*b*), including the statistical errors on the distribution. The scattering contrast was set to $\Delta\rho = 4.00 \times 10^{10}$ cm^{-2}. The fit to the experimental data was good and the distribution agrees reasonably with the one determined by Pedersen (1993*a*). However, the large-R part of the distribution has a tail extending beyond 40 Å, which was not found using the Weibull distribution. The parameters derived from the size distribution are given in Table 6, which also contains the results of applying the model with a Weibull size distribution. The derived parameters agree reasonably except for the radii of gyration, which deviate by about 20% owing to the difference of the size distributions at large R values.

The fit of the analytical model to the data is shown as the curve in Fig. 9(*a*). The fit to the data is satisfactory. The size distribution is shown in Fig. 9(*b*). It deviates somewhat from the one determined by the local monodisperse model and is nearly identical to the one obtained using the Weibull distribution (Pedersen, 1993*a*). The parameters derived from the distribution

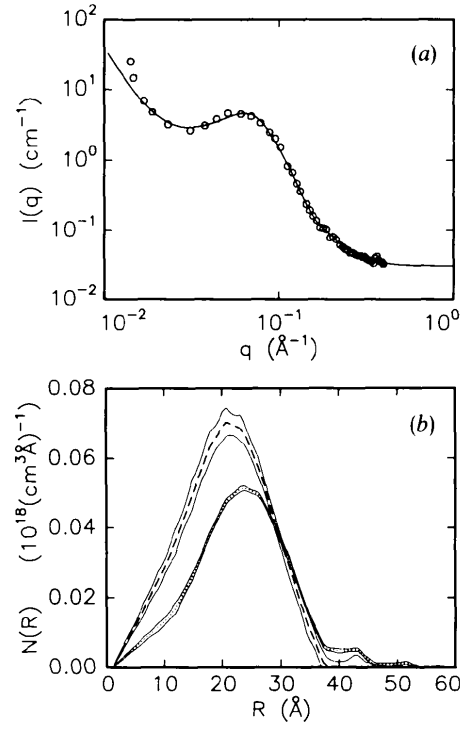

Fig. 9. (*a*) Experimental scattering data from Triolo *et al.* (1989) for Al–2.14 wt%Li. (*b*) The size distributions. The dotted curve is from the local monodisperse approximation and the broken curve is from the analytical model. The light full curves show the statistical errors.

Table 6. *Results from the analysis of the experimental scattering data shown in Fig. 9 (Triolo et al., 1989) for* Al–2.14 wt%Li

The parameters describing the interference effects are: for the local monodisperse approximation, $C = 1.23$ and $\eta_{HS} = 0.34$; for the analytical model, $C = 1.53$ (1). The scattering contrast was $\Delta\rho = 4.0 \times 10^{10}$ cm^{-2} for the local monodisperse model and $\Delta\rho = 4.0$ (4) $\times 10^{10}$ cm^{-2} for the analytical model. The parameters for the Weibull distribution (Pedersen, 1993*a*) are $C = 1.49$ (3) and $\Delta\rho = 3.92$ (12) $\times 10^{10}$ cm^{-2}.

Parameters	Local monodisperse	Analytical	Weibull
$\overline{R}$ (Å)	23.4 (2)	20.4 (7)	21.5 (5)
$\sigma(R)$ (Å)	8.3 (1)	7.3 (6)	6.7 (2)
R_{gyr} (Å)	30.6 (1)	23.4 (37)	23.8 (3)
η	0.076 (1)	0.067 (11)	0.070 (5)
S (cm^{-1})	787000 (5000)	803000 (131000)	827000 (51000)

are given in Table 6. There is good agreement between the results from the analytical model and those from the Weibull distribution model. Note also that the compositions of the aluminium matrix and of the precipitates can be calculated from the scattering-length density (Pedersen, 1993*a*). The values agree well with the known solubility limit and the expected composition of Al_3Li of the δ' precipitates.

6. Summary and concluding remarks

The analysis of small-angle scattering data for polydisperse systems with hard-sphere interactions has been discussed. A new approximation for calculating the scattering intensity has been introduced. Within this approximation, the scattering intensity is given as that of a system that is locally monodisperse. Comparisons with model calculations using the analytical expressions of Vrij (1979) show that the local monodisperse approximation gives reasonable results for volume fractions up to about 0.4 and for large polydispersities. Comparisons with model calculations using the 'decoupling approximation' (Kotlarchyk & Chen, 1983) show that the local monodisperse approximation gives results that agree much better with the analytical model for high volume fractions and large polydispersities. In the local monodisperse approximation, the approximations made in (14) and the use of (15) for the structure factor account reasonably for the effect of polydispersity on the effective structure factor. This is because the influence of polydispersity of the interaction radius is to a certain degree taken into account. In the decoupling approximation, the structure factor is approximated by that of a monodisperse system multiplied by a factor $[\overline{\beta(q)}]$ that takes into account the influence of polydispersity of the form factors. This means that the polydispersity of the interaction radius is not considered in the decoupling procedure. Although this effect is only included in an approximation in the local monodisperse approximation, it is sufficient to give a much better agreement with the analytical results.

An additional advantage of the local monodisperse approximation is that the scattering intensity is linearly dependent on the amplitude of the size distribution. For free-form determination of the size distribution using a spline parameterization of the size distribution and a constrained least-squares method, this means that the least-squares problem is linear in the parameters describing the amplitude of the size distribution. This makes the computations reasonably fast. The two parameters describing the effective structure factors of the systems are optimized in an external nonlinear routine. (For a typical data set it takes less than one minute on a workstation.) The constraints in the linear least-squares problem are a non-negativity constraint and a smoothness constraint.

The analysis of simulated examples for relatively large volume fractions and large polydispersities shows that the local monodisperse model gives reasonable estimates of the size distribution. Some systematic errors are occasionally present at large R values, owing to the approximate nature of the structure factor, which influences the scattering intensity at small q values.

Application of the analytical expressions of Vrij (1979) gives scattering intensities that are strongly nonlinearly dependent on the amplitude of the size distribution. With a nonlinear least-squares routine with smoothness and non-negativity constraints, the analytical expressions were also used for determining free-form size distributions expressed as linear combinations of spline functions. The input parameters are taken from the fit of the local monodisperse model. The typical time for a calculation, including the variation of the weight of the smoothness constraint, is 5–10 min. The application to simulated data shows that the analytical model gives very good estimates of the original size distributions. The smoothness constraint gives rise to some smearing of the size distribution at small R values. The fits are not very sensitive to the smaller particles, owing to the weighting of the intensity (at $q = 0$) with the volume squared of the particles. For the analytical model, the characteristic parameters derived from the size distribution agree to typically better than 10% with the original values.

The application of the models to real experimental data showed that useful information on the size distribution can be obtained even for samples with a very high hard-sphere volume fraction. For the silica particles with a relatively low polydispersity, the agreement between the two models, as well as with electron microscopy, is very good even for a volume fraction as high as 0.5. For the Al–Li sample, the size distributions from the local monodisperse model and from the analytical model deviate significantly. However, the parameters derived from the size distribution agree reasonably.

The models and methods are presently being applied to the scattering data from krypton bubbles in copper

(Pedersen, Eldrup & Horsewell, 1994) and from γ' precipitates in Ni–Ti (Vyskocil, Schönfeld, Pedersen & Kostorz, 1994) and Ni–Al–Mo (Calderon & Kostorz, 1991; Calderon, Pedersen & Kostorz, 1994; Sequeira, Calderon, Pedersen & Kostorz, 1994). Comparison with electron microscopy shows good agreement for the size distributions.

Stimulating discussions with M. Eldrup, S. Hansen, K. Mortensen, A. D. Sequeira, P. Vyskocil, H. Calderon and G. Kostorz are gratefully acknowledged. I thank A. N. Falcão, S. Hansen, K. Mortensen and D. I. Svergun for valuable comments on the manuscript.

References

BEVINGTON, B. R. (1969). *Data Reduction and Error Analysis for the Physical Sciences*. New York: McGraw-Hill.

BLUM, L. & STELL, G. (1979). *J. Chem. Phys.* **71**, 42–46; erratum (1980), **72**, 2212.

CALDERON, H. & KOSTORZ, G. (1991). *Proceedings of the Morris E. Fine Symposium*, edited by P. K. LIAW, J. R. WEERTMAN, H. R. MARCUS & J. S. SANTNER, pp. 11–16. Warrendale, PA: The Minerals, Metals and Materials Society.

CALDERON, H. A., PEDERSEN, J. S. & KOSTORZ, G. (1994). In preparation.

FRATZL, P. (1991). *J. Appl. Cryst.* **24**, 593–597.

GLATTER, O. (1977). *J. Appl. Cryst.* **10**, 415–421.

GLATTER, O. (1980). *J. Appl. Cryst.* **13**, 7–11.

KALER, E. (1988). *J. Appl. Cryst.* **21**, 729–736.

KINNING, D. J. & THOMAS, E. L. (1984). *Macromolecules*, **17**, 1712–1718.

KOSTORZ, G. (1991). *J. Appl. Cryst.* **24**, 444–456.

KOTLARCHYK, M. & CHEN, S.-H. (1983). *J. Chem. Phys.* **79**, 2461–2469.

KRUIF, C. G. DE, BRIELS, W. J., MAY, R. P. & VRIJ, A. (1988). *Langmuir*, **4**, 668–678.

LAWSON C. L. & HANSON, R. J. (1974). *Solving Least Squares Problems*. New Jersey: Prentice-Hall.

LI, Q., KESTERNICH, W., SCHROEDER, H., SCHWAHN, D. & ULLMAIER, H. (1990). *Acta Metall. Mater.* **38**, 2383–2392.

MAHALINGAM, K., GU, B. P., LIEDL, G. L. & SANDERS, T. M. JR (1987). *Acta Metall.* **35**, 483–498.

MARQUARDT, D. W. (1963). *J. Soc. Ind. Appl. Math.* **11**, 431–441.

OTTEWILL, R. H. (1991). *J. Appl. Cryst.* **24**, 436–443.

PEDERSEN, J. S. (1992). *J. Appl. Cryst.* **25**, 129–145.

PEDERSEN, J. S. (1993*a*). *Phys. Rev. B*, **47**, 657–665.

PEDERSEN, J. S. (1993*b*). *J. Phys.* II (*Paris*) *Colloq.* C8, **3**, 491–498.

PEDERSEN, J. S., ELDRUP, M. & HORSEWELL, A. (1994). In preparation.

PEDERSEN, J. S., POSSELT, D. & MORTENSEN, K. (1990). *J. Appl. Cryst.* **23**, 321–333.

POTTON, J. A., DANIELL, G. J. & RAINFORD, B. D. (1988). *J. Appl. Cryst.* **21**, 663–668, 891–897.

PRESS, W. H., FLANNERY, B. P., TEUKOLSKY, S. A. & VETTERLING, W. T. (1989). *Numerical Recipes*. Cambridge Univ. Press.

PROVENCHER, S. W. (1982). *Comput. Phys. Commun.* **27**, 213–227.

SALACUSE, J. J. & STELL, G. (1982). *J. Chem. Phys.* **77**, 3714–3725.

SCHNABLEGGER, H. & GLATTER, O. (1991). *Appl. Optics*, **30**, 4889–4896.

SEQUEIRA, A. D., CALDERON, H. A., PEDERSEN, J. S. & KOSTORZ, G. (1994). In preparation.

SVERGUN, D. I. & PEDERSEN, J. S. (1994). *J. Appl. Cryst.* **27**, 241–248.

SVERGUN, D. I., SEMENYUK, A. V. & FEIGIN, L. A. (1988). *Acta Cryst.* A**44**, 244–250.

TRIOLO, R., CAPONETTI, E., SPOONER, S. & BOSCHETTI, F. (1989). *Philos. Mag.* A**60**, 401–414.

VRIJ, A. (1979). *J. Chem. Phys.* **71**, 3267–3270.

VYSKOCIL, P., SCHÖNFELD, B., PEDERSEN, J. S. & KOSTORZ, G. (1994). In preparation.